Article citation info:
ESTRADA Q, SZWEDOWICZ D, MAJEWSKI T, MARTINEZ E, RODRIGUEZ-MENDEZ A. Effect of quadrilateral discontinuity size on the energy absorption of structural steel profiles. Eksploatacja i Niezawodnosc – Maintenance and Reliability 2016; 18 (2): 186–193, http://dx.doi.org/10.17531/ein.2016.2.5.

Quirino ESTRADA
Dariusz SZWEDOWICZ
Tadeusz MAJEWSKI
Eladio MARTINEZ
Alejandro Rodriguez-MENDEZ

EFFECT OF QUADRILATERAL DISCONTINUITY SIZE ON THE ENERGY ABSORPTION OF STRUCTURAL STEEL PROFILES

WPŁYW WIELKOŚCI CZWOROBOCZNYCH NIECIĄGŁOŚCI NA POCHŁANIANIE ENERGII W STALOWYCH PROFILACH STRUKTURALNYCH*

In this paper the effect of discontinuity size on energy absorption performance of steel square profiles is reported. The analysis consists of finite element simulations and experimental results of the compression strength of steel profiles with discontinuities. The discontinuities were placed at the mid span of the profiles in two walls opposite to each other. Square, rectangular and diamond initiators were evaluated at different scales. The numerical results determined the size intervals that present a good energy absorption performance in each case. Energy absorption capabilities were increased up to 12.54% with respect to a structure without discontinuities. Additionally, the peak load value (P_{max}) was decreased 25.97% with the implementation of a diamond initiator. For structures with discontinuities with major axis close to the profile width, a buckling effect was observed. Finally, it was observed that the size of the initiators contributes to reduce the peak load (P_{max}) value.

Keywords: *thin-walled structure, geometrical discontinuities, finite element method, energy performance.*

W pracy przedstawiono analizę wpływu rozmiaru nieciągłości na pochłanianie energii przez stalowe profile o przekroju kwadratowym. Analiza przedstawia wyniki symulacji elementami skończonymi próby ściskania profili stalowych z nieciągłościami oraz porównanie z danymi eksperymentalnymi. Nieciągłości zostały usytuowane w środku profilu w dwóch przeciwległych ścianach. W pracy zostały przebadane nieciągłości o formach kwadratowych, prostokątnych i rombowych dla różnych wymiarów. Stwierdzono wzrost o 12,54% możliwości pochłaniania energii w porównaniu dla struktur bez nieciągłości. Dodatkowo, w przypadku nieciągłości rombowych stwierdzono spadek wartości siły maksymalnej (Pmax) o 25,97%. Zaobserwowano występowanie efektu wyboczenia dla nieciągłości rombowej gdy wymiar jej osi zbliża się do szerokości profilu. Zaobserwowano, ze rozmiar nieciągłości wpływa na redukcje wartości maksymalnego obciążenia oraz w tym samym czasie na obniżenie pochłanianej energii.

Słowa kluczowe*: struktury cienkościenne, nieciągłości geometryczne, metoda elementów skończonych, pochłanianie energii.*

1. Introduction

Worldwide, an estimated of 1.2 million people die in road crashes every year and 50 million are injured. This evidence can be increased by 65% for the next 20 years [16]. With the introduction of the crashworthiness concept in previous decades and the addition of the efforts to ensure the life of the passengers, the use of thin walled structures as energy passive absorbers is taking relevance. Many characteristics can be attributed to them; however, the most important is the high performance which absorbs energy by plastic deformation. With the objective to optimize the energetic behavior of structural members, numerical and experimental studies have been realized. In these studies, factors such as cross section geometry [21, 11], length of the profile [10] and manufacture material [17] have been evaluated. Other studies have focused their efforts in the implementation of geometrical discontinuities to reduce the peak load value. Many shapes of imperfections have been analyze such as circular [2, 4, 5], slotted [13], elliptical [9] and dimples [8]. In all cases the effectiveness of discontinuities have been corroborated, nevertheless according to Szwedowicz et al [18] the energy abortion capacity also can be modified by location of imperfections along the structure. In [14] the effect of location of circular discontinuities on square profile was studied, concluding that the best performance is obtained by placing discontinuities at middle height. Likewise, a numerical comparison between circular, elliptical and slotted discontinuities was carried out by [6]. In the analysis the initiators were located at the midpoint of the square aluminum tube in two opposite walls. A reduction of 11.7% in peak load value was obtained with a pair of holes. In this paper the effect of discontinuity size on the crashworthiness characteristics of square steel profiles is analyzed. For this purpose, numerical simulations were realized using Abaqus finite element software. Square, rectangular and elliptical geometries discontinuities were evaluated at difference scales.

(*) Tekst artykułu w polskiej wersji językowej dostępny w elektronicznym wydaniu kwartalnika na stronie ***www.ein.org.pl***

2. Measurement of the energy absorption performance

As mentioned there are two important parameters to determine the response of structural members under crushing force; the energy absorbed (E_a) and the maximum value of crushing load called peak load (P_{max}). The energy absorption by elastic and plastic deformation can be calculated by integration of the area below the load-displacement curve, using the following equation [7]:

$$E_a = \frac{1}{2}\sum_{i}^{n-1}\left(F(\delta)_{i+1} + F(\delta)_i\right)\cdot(\delta_{i+1} - \delta_i) \quad (1)$$

where: F is the crushing force and δ is the displacement in the axial direction.

After reaching the P_{max} value, the initial stiffness of the structure is broken. Then the force required to continue with plastic deformation decreases with an oscillating value. This force is denominated mean crushing force and it is equal to the ratio of the absorbed energy (E_a) and displacement (δ) [7]:

$$P_m = \frac{E_a}{\delta} \quad (2)$$

A dimensionless parameter that associates the energy absorbed (E_a), the peak load (P_{max}) value and the displacement (δ) is known as the energy efficiency (E_e) defined by [19], is expressed in %:

$$E_e = \frac{E_a}{P_{\max}\cdot\delta}\cdot 100\% \quad (3)$$

Finally the specific energy (S_e) is used when the structures evaluated have different mass. It is defined as the ratio of energy absorbed (E_a) to the mass (m) of the structure [12]:

$$S_e = \frac{E_a}{m} \quad (4)$$

3. Numerical model and experimental validation

A first numerical model about the crushing process of a steel square profile without discontinuities was developed in Abaqus/Explicit. The geometry evaluated corresponds to a structure with square cross-section (50 x 50 mm), 240 mm in length, thickness of 1.32 mm and rounded corners (radius of 2 mm). According to [3, 18] and in addition with the quasi-static nature of the compression test, the profile was modeled with elastic-plastic material properties and the hardening effects were negated. The structural member was modeled as a deformable body with shell elements (S4R) with a thickness of 1.32 mm. The crushing process was carried out by two rigid plates using R3D4 elements. A fixed displacement restriction was applied to a lower plate while an upper rigid plate could move only in the y- direction to allow the compression of the structure. The boundary conditions applied to a profile were a tie restriction between the upper tip and the lower rigid plate beside a contact interaction between the upper tip and the top rigid plate. Finally a general contact condition was established to ensure the internal and external contact during the forming of wrinkles. A frictional coefficient of 0.15 was used for all contact conditions. A smooth post-buckling response was introduced in the discrete model by the *IMPERFECTION command. In this sense were introduced first two eigenvalues with an imperfection sensivity equal to 0.1 of thickness value. The eigenvalues were obtained from buckle analysis in Abaqus. The elastic-plastic properties of the material were established using an isotropic plasticity model. The mechanical properties of the material used for the development of the numerical model, were [15]: Young modulus = 200 GPa, Poisson's ratio = 0.26, yield stress = 250 MPa, density = 7850 kg/m^3. The hardening effects due to the load velocity were not considered in the discrete models.

The numerical model of the structure was validated experimentally by a quasi-static crushing test. The structural member was subjected to compression load by universal test machine (Shimadzu UH-300 kNI) with a velocity of 6 mm/min. During the evaluation test, the profile was located between two compression plates, after a maximum displacement of 160 mm was programmed. The figures 1, 2, 3 and 4 show the mechanical behavior of the profile to compare numerical and experimental results. In all cases a good agreement it was obtained. In this form the usefulness of the discrete model of the test specimen was experimentally validated and it was used to modeling discontinuities.

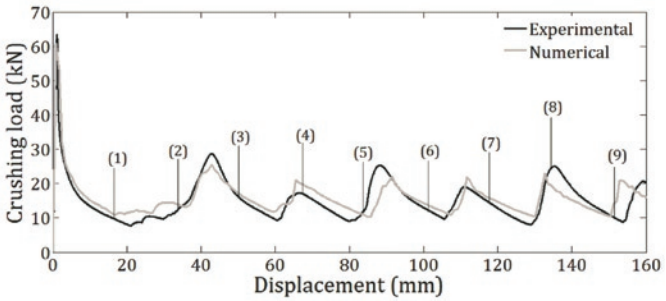

Fig. 1. Comparison of numerical and experimental load/displacement curves

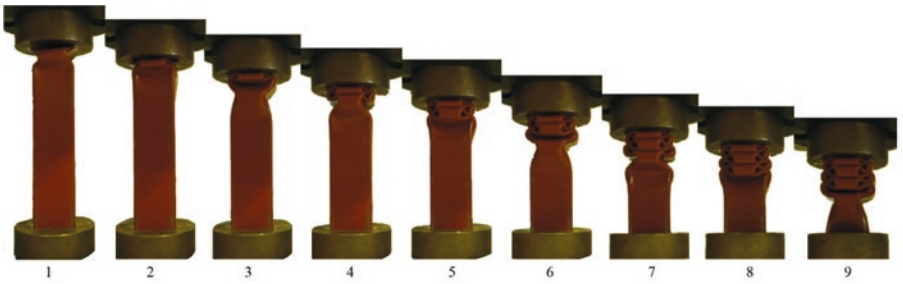

Fig. 2. Progressive collapse of specimen ST-01 (without holes)

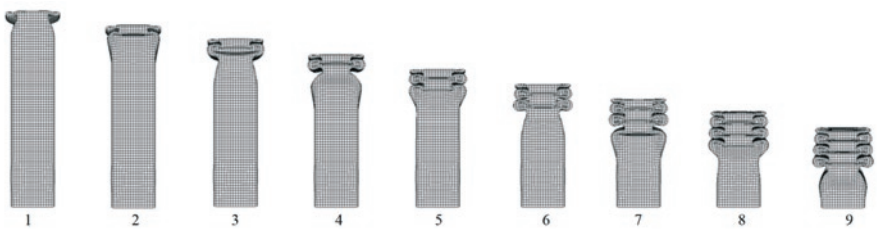

Fig. 3. Numerical simulation of the progressive collapse process of specimen ST-01 (without holes)

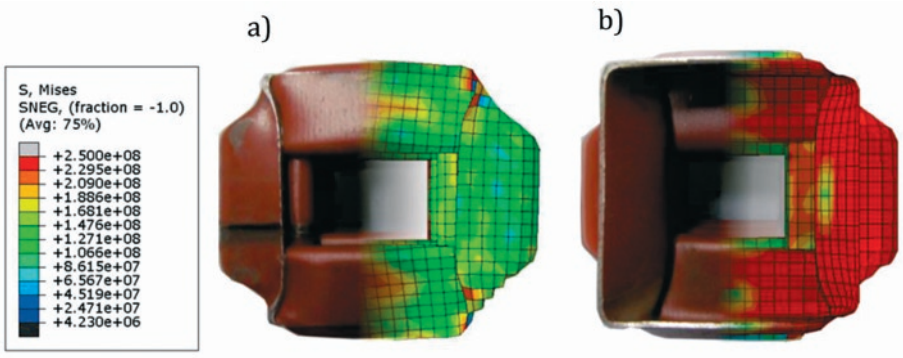

Fig. 4. Experimental and numerical final deformation state for the straight square profile (ST-01), where: a) top view and b) bottom view, S in MPa

4. Development of numerical simulation with discontinuities

The effect of discontinuity size on the response of square structures is evaluated by means of several numerical models. Since the best position to bore imperfections is at the mid span of the specimen walls in symmetric arrangements [14, 18], square, rectangular and diamond discontinuities were placed at mid span on the structure in two opposite walls (120 mm). The initial sizes of the imperfections were determined from the Von Karman principle based on effective width. In this way the implementation of the discontinuity modifies the mechanical response of the structure.

The structures were divided in three groups depending on the shape of the discontinuity. In each case, the discontinuity size was increased by a scale factor; this factor defines the resizing rate of the discontinuities in respect to the smallest size of the initiator for every group. The geometry of the structures is given in Table 1 for groups I, II and III, respectively.

Table 1. Geometry employed in group I, II, III

Group I. Geometrical details				
Profile code	Shape of discontinuity	Size of discontinuity (mm) Side	Scale Factor	Mass (gr)
I-A	Square	5.32	-	477.94
I-B		7.98	1.50	477.21
I-C		10.63	2.00	476.18
I-D		13.29	2.50	474.86
I-E		15.95	3.00	473.25
I-F		18.61	3.50	471.35

Group II. Geometrical details					
Profile code	Shape of discontinuity	Size of discontinuity (mm) Major axis (horizontal)	Minor axis (vertical)	Scale Factor	Mass (gr)
II-A	Rectangular	6.65	4.25	-	477.94
II-B		9.97	6.38	1.50	477.21
II-C		13.29	8.51	2.00	476.18
II-D		16.62	10.63	2.50	474.86
II-E		19.94	12.76	3.00	473.25
II-F		23.26	14.89	3.50	471.35

Group III. Geometrical details					
Profile code	Shape of discontinuity	Size of discontinuity (mm) Major axis (horizontal)	Minor axis (vertical)	Scale Factor	Mass (gr)
III-A	Diamond	9.40	6.02	-	477.94
III-B		14.10	9.02	1.50	477.21
III-C		18.80	12.03	2.00	476.18
III-D		23.50	15.04	2.50	474.86
III-E		28.20	18.05	3.00	473.25
III-F		32.90	21.06	3.50	471.35

5. Results and discussion

5.1. Group I. Square discontinuities

The crushing behaviour of structures in group I was obtained by force-displacement curves, which are presented in figures 5 and 6. The crushing load and plastic folds of structures I-A, I-B and I-C present similar behaviours. Even if the mechanical response of the structures were similar, small differences are found at P_{max} due to the size of discontinuities. After reaching the peak value ($P_{max)}$, the crushing load continues to deform the material with a mean crushing force of 17.62 kN. Besides at displacement of 110 mm, a second increase of crushing load is produced.

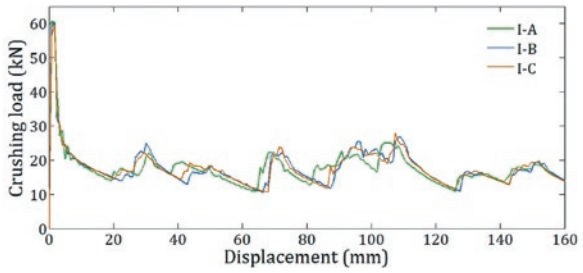

Fig. 5. Load–displacement curves for structure with square discontinuities (first part)

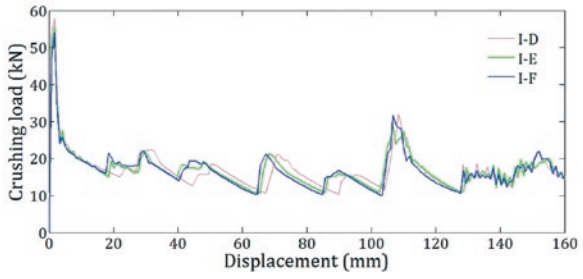

Fig. 6. Load–displacement curves for structure with square discontinuities (second part)

In respect to profiles I-D, I-E and I-F, the effect of size on P_{max} has a better appreciation. A decrease of this value was noticed by increasing the size of the initiators. The mean crushing force (P_m) for these profiles presents an approximated value of 16.87 kN. This means a decrease of P_m with respect to the first structures. Small differences occurred during the plastic fold mechanism, although the appearing of a second pulse of crushing load was presented in all cases, at a displacement of 105 mm (see figure 6).

The energy absorption capacities of the profiles depend on the quantity and mode of deformation. The absorbed energy occurs in

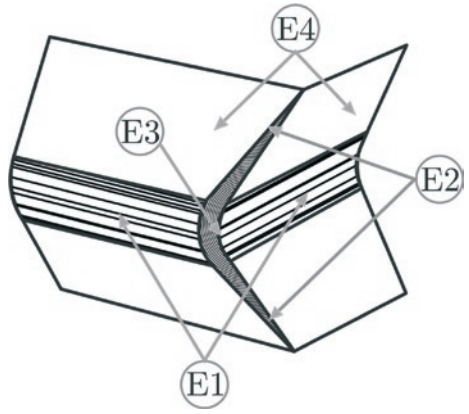

Fig. 7. Forming of plastic surfaces at basic folding mechanism element [20]

Fig. 8 Effect of size of discontinuities on formation hinge lines for group I

four different ways by the formation of cylindrical (E1), conical (E2), toroidal (E3) and trapezoidal surfaces (E4), (see figure 7). For all analysed structures, the formation of plastic wrinkles was determined by localization of the discontinuity. Additionally, it was observed, that as the size of discontinuities increases, the formation of hinge lines presents low resistance on collapsing, in this way the peak load value diminished (see figure 8). However, the size of discontinuities was increased; a buckling effect appeared at the vicinity of the discontinuity, causing just a partial deformation in the structure.

After the first wrinkle was created, the structures showed two different ways of fold formation. Some structures were deformed with direction to the upper tip of the profile (e.g. I-A) and others continued to the bottom tip profile (e.g. I-D). The final deformation state for all structures is shown in figure 9. The global collapse mode of the structures was symmetric (s), independent of the hole´s size. A summary of the performance of the structures belonging to the group I is shown in Table 2. In all cases, the P_{max} value decreases within a range of 0.77–11.55% compared with a profile without discontinuities (ST-01). The energy absorbed increased until reaching a maximum value of 2.84 kJ (I-C), later an increase in the scale factor produced a reduction of energy absorption in structures I-D, I-E and I-F. The largest energy efficiency (E_e) was obtained for the profile named I-F with a value of 31.12%, a value close to 100% represents the optimal efficiency of the structure. Due to the quasi-static nature of the compression test simulation and the symmetry of the discontinuities, the final deformation state of the specimens, was symmetric (s).

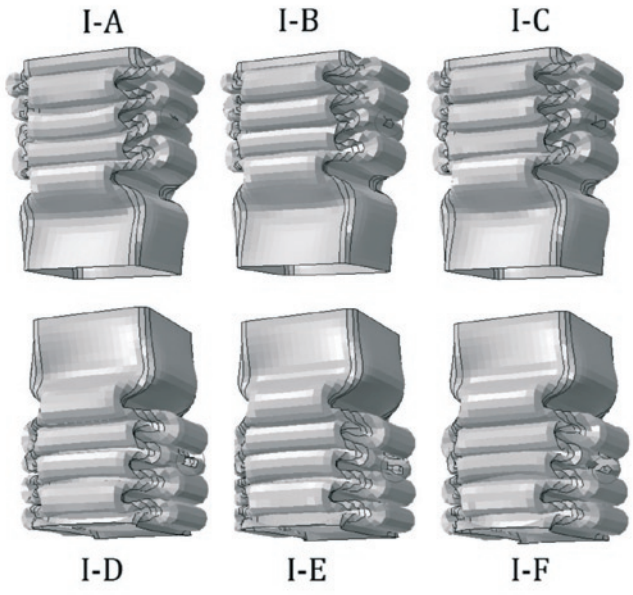

Fig. 9. Final deformation state for profiles with square discontinuities

Table 2. Numerical results for group I.

Profiles with square discontinuities (group I)						
Specimen code	P_{max} (kN)	P_m (kN)	E_a(kJ)	E_e(%)	S_e(J/gr)	Deformation mode
ST-01	61.03	15.94	2.55	26.11	5.32	s
I-A	60.56	17.69	2.83	29.21	5.92	s
I-B	59.99	17.68	2.82	29.47	5.93	s
I-C	59.70	17.77	2.84	29.77	5.97	s
I-D	57.87	16.93	2.70	29.25	5.70	s
I-E	55.40	16.96	2.71	30.61	5.73	s
I-F	53.98	16.80	2.68	31.12	5.70	s

5.2. Group II. Rectangular discontinuities

The crushing load vs displacement curves for these profiles are shown in figures 10 and 11. A perceptible difference was noticed between the profile II-A and II-B. Moreover, structures II-B and II-C described a similar crushing behaviour during the plastic deformation process. The peak load (P_{max}) at the beginning of the compression process was diminished by increasing the size of the discontinuity.

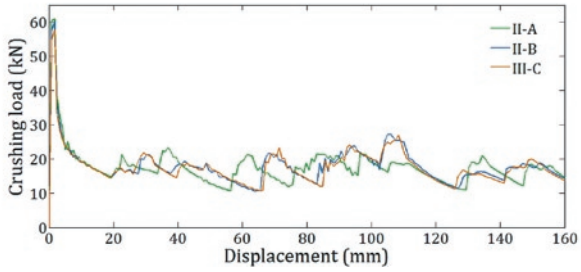

Fig. 10. Load–displacement curves for structures with rectangular discontinuities (first part)

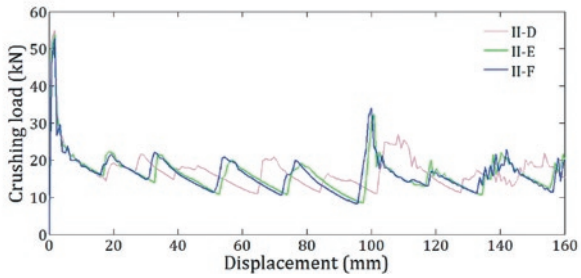

Fig. 11. Load–displacement curves for structure with square discontinuities (second part)

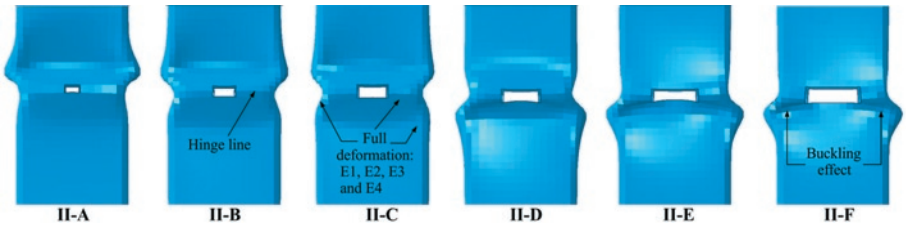

Fig. 12. Effect of size of rectangular discontinuities on formation hinge lines for group II

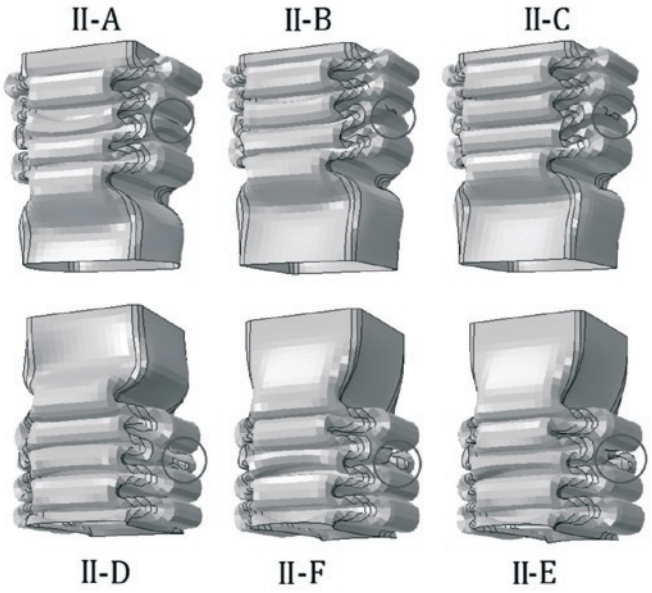

Fig. 13. Final deformation state for profiles with rectangular discontinuities.

Table 3. Numerical results for group II

Profiles with rectangular discontinuities (group II)						
Specimen code	P_{max} (kN)	P_m (kN)	E_a(kJ)	E_e(%)	S_e(J/gr)	Deformation mode
ST-01	61.03	15.94	2.55	26.11	5.32	s
II-A	61.08	17.60	2.81	28.81	5.89	s
II-B	60.00	17.88	2.86	29.79	5.99	s
II-C	57.81	17.74	2.83	30.68	5.96	s
II-D	54.88	17.09	2.73	31.14	5.76	s
II-E	53.78	16.44	2.63	30.57	5.56	s
II-F	52.81	16.40	2.62	31.05	5.57	s

The tendency of reduction of the peak load continues to appear for structures II-D, II-E and II-F. Very close mechanical behaviours are described by profiles II-E and II-F, particularly during the emergence of an increase in the crushing load at approximately 97 mm. This increase in crushing load is due to a change in the direction of the formation of the plastic folds. The mean crushing force (P_m) for II-E and II-F presented similar values during the plastic deformation process with an approximate value of 16. 42 kJ.

According to numerical simulations, effects such as the formation of hinge lines during the first plastic wrinkles and the energy absorption capabilities (E_a), are directly associated to the size of the discontinuities. The energy absorption occurs by plastic deformation of the structure (see figure 7). An increase on the discontinuity size generates a buckling effect at the near regions of the discontinuity. This effect provokes a reduction of the peak load and at the same time a reduction of the energy absorption capacity was observed due to a partial deformation of the structure (see figure 12).

After the collapse of the structure for the first time, the plastic deformation process was propagated in two directions, one at a time, depending on the hinge line formation. Consequently, all the material was deformed in one direction, the process repeats in the opposite direction until reaching the final state of deformation. The structures showed symmetric collapse modes independent of the size of the hole (see figure 13).

Table 3 presents the results obtained for the profiles in group II. Accordingly, as the scale factor is increased, the P_{max} values decrease to around 1.69-13.47% with respect to a structure without holes (ST-01). Also, the energy absorbed (E_a) increases until it reaches a maximum value of 2.86 kJ (12.15%) for the structure II-B. Later the profiles showed a gradual decay of performance on E_a by the resizing of discontinuities. The largest energy efficiency (E_e) was registered by profile II-D with a value of 31.14%. A symmetric collapse mode was observed in all the profiles evaluated.

5.3. Group III. Diamond discontinuities

The load–displacement curves for structures with diamond shape discontinuities are presented in figures 14 and 15. According to these results, the size of the discontinuities did not modify the behaviour of structure III-B compared to III-A. Regarding to profile III-C, a second major value of peak load was noticed at a 100 mm displacement. This increase of peak load is due to a change in the direction of the formation of wrinkles.

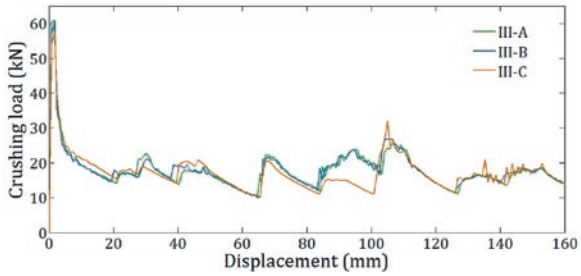

Fig. 14. Load–displacement curves for structure with diamond discontinuities (first part)

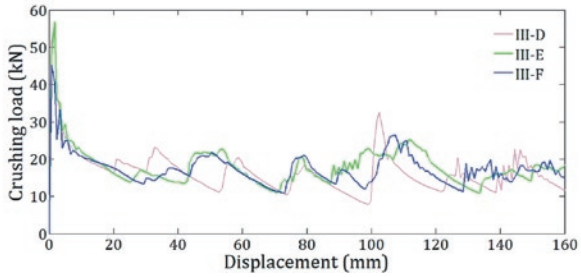

Fig. 15. Load–displacement curves for structure with diamond discontinuities (second part)

The effect of size of the diamond-shape hole on peak load (P_{max}) projected from the structure III-F, where a reduction of peak load (P_{max}) was obtained with respect to structures III-D and III-E, which show similar peak load values. The crushing response of the structures presents similar loops, however when the mean crushing force (P_m) was calculated, some differences were found. Thus, the mean

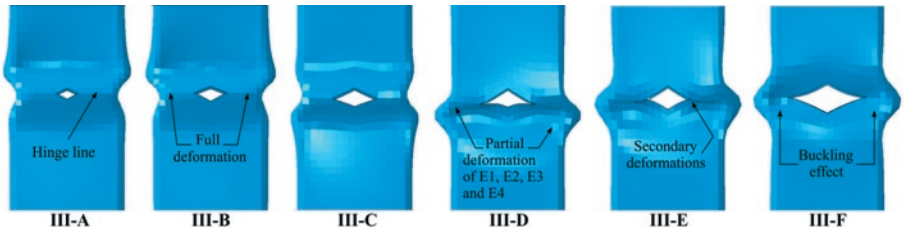

Fig. 16. Effect of size of diamond discontinuities on formation hinge lines for group III

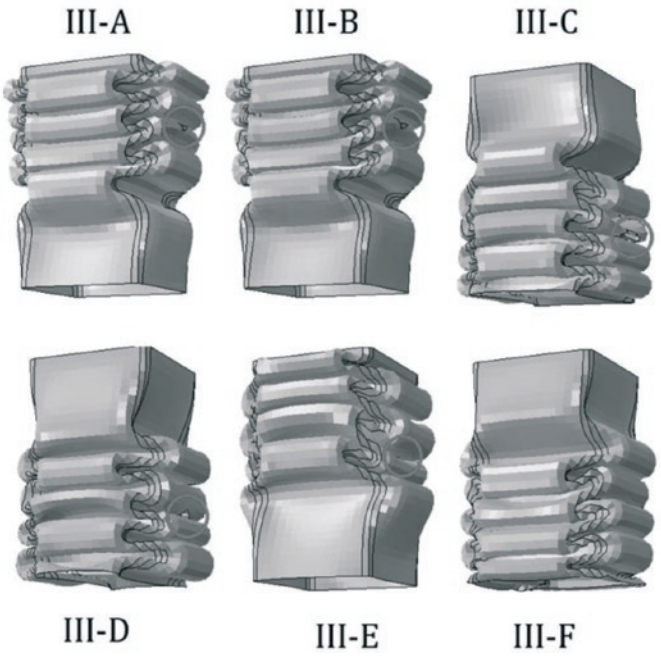

Fig. 17. Final deformation state for profiles with diamond discontinuities

crushing force values were 16.56, 17.94 and 17.34 kN for structures III-D, III-E and III-F, respectively.

The formation of hinge lines was determined by the location of the discontinuity. In this part, the crushing load required for its formation depended on the size of the discontinuities, decreasing as the scale factor increased. During the creation of the external cylindrical face (E1) the structure III-A and III-B showed a full deformation of material while it was partially interrupted in structure III-C, contributing to diminish the energy absorption performance (see figure 16). For structures with discontinuities of length of major axis, close to the width of the profile, the formation of the external and internal cylindrical faces was interchanged (III-D, III-E and III-F).

The final deformation state of the structures with diamond shape holes is shown in figure 17. Despite the fact that the profile described

Table 4. Numerical results for group III

Profiles with diamond discontinuities (group III)						
Specimen code	P_{max} (kN)	P_m (kN)	E_a(kJ)	E_e(%)	S_e(J/gr)	Deformation mode
ST-01	61.03	15.94	2.55	26.11	5.32	s
III-A	60.93	17.84	2.85	29.23	5.97	s
III-B	60.16	17.92	2.86	29.71	6.01	s
III-C	57.32	17.32	2.77	30.20	5.82	s
III-D	55.72	16.56	2.64	29.61	5.58	s
III-E	56.82	17.94	2.87	31.57	6.06	s
III-F	45.18	17.34	2.77	38.32	5.89	s

different directions of propagation after the first collapse; the complete structure reached symmetric modes of deformation.

A summary of the results obtained is given in Table 4. According to these results, the peak load (P_{max}) decreases as the size of the discontinuities increases. The minimum value of P_{max} reached was 45.18 kN for structure III-F, this quantity represents a decrease of 25.97% respect to a square profile without discontinuities (ST-01). A maximum value of energy absorbed of 2.87 kJ (12.54%) was obtained by III-E, this means a good relation of specific energy (S_e) of 6.06 J/gr. However, according to E_e, the structure III-F presented the best energetic performance with a value of 38.32 %. Finally a symmetric (s) mode of deformation was observed in all structures evaluated.

5.4. Discussion of results

In order to visualize the response of the structures due to variation of geometry and initiator's size, a comparison of peak load (P_{max}) values for all structures is presented in figure 18. If the outlier value for structure III-E is neglected, a tendency of reduction in the peak load due to an increase in size of the discontinuity is observed. For structures with denomination A and B (Groups I, II and III) the value of P_{max} was independent of the initiator geometry. The geometrical factor gains importance in the structures with denomination C.

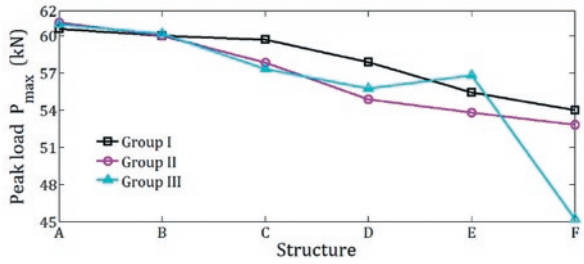

Fig. 18. Comparison of P_{max} values obtained for different groups of structures

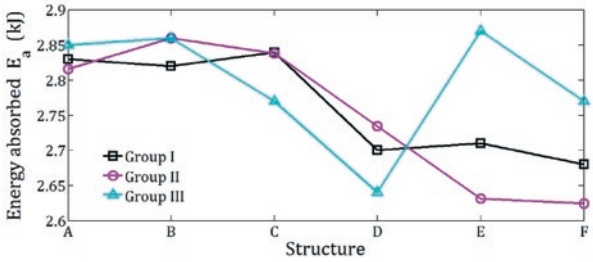

Fig. 19. Comparison of energy absorbed for different groups

Independently of geometry of holes a reduction of energy absorbed performance was noticed for groups I and II (profiles with square and rectangular initiators). In this way a maximum value of 2.84 kJ and 2.86 kJ was obtained for profiles I-B and II-B, respectively. The structures with diamond discontinuities (Group III) followed the same tendency of decrease of structure D. Subsequent profiles III-E and III-F show a secondary effect that caused an increase of energy absorption (see figure 19).

The increase of energy absorption characteristics, contrary to what is expected for specimens III-E and III-F, is directly associated with the mode of formation of the first wrinkle. Figures 20 is presented where the size of discontinuities causes torsional effects (2) along the major axis of the initiator, furthermore, a movement of inward curl

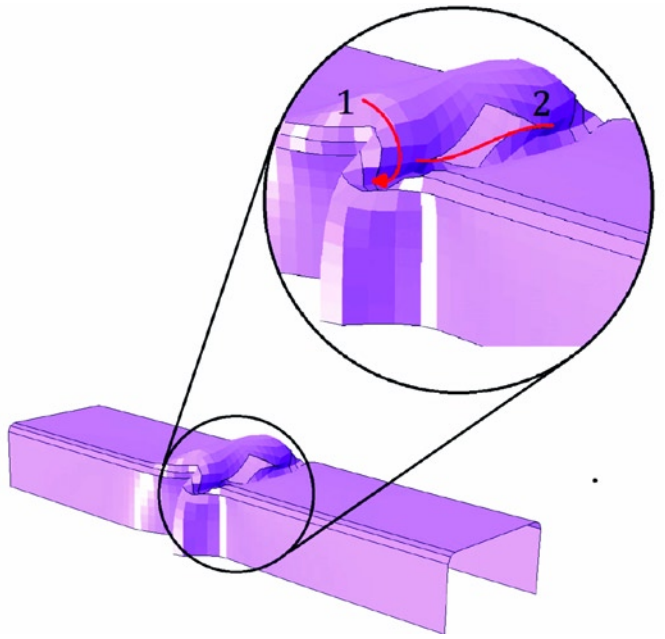

Fig. 20. Secondary effects by increase the size of the discontinuity in profile III-E

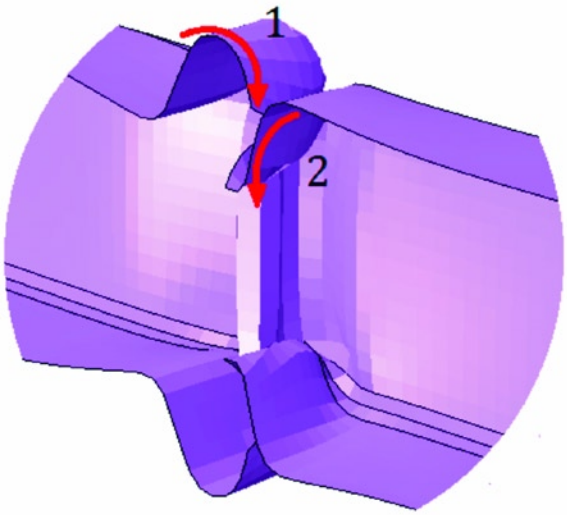

Fig. 21. Secondary effects by increase the size of the discontinuity in profile III-E

was developed (1), both effects contribute to increase the energy absorption performance.

Finally, with a cut view of profile III-E, a third mechanism of energy absorption is exposed, which indirectly improves the performance of the profile. After the inward curl process is completed (1), a contact between folds (external and internal) is presented. It produces additional work to deform the inner wrinkle counterclockwise (3), such as seen in figure 21.

Finally according to figure 19 for the specific case of this paper, there is a maximum energy value that can be absorbed by the structures suggesting a limit for the sizing of the discontinuities. In this way the limits related to the sizing of the square, rectangular and diamond discontinuities were numerically found according to the width of structure C, side (S) and the length of the major axis of the discontinuity (D).

For square discontinuities:

$$0.10C \leq S \leq 0.21C$$

For rectangular discontinuities:

$$0.13C \leq D \leq 0.27C$$

For diamond discontinuities:

$$0.19C \leq D \leq 0.28C$$

5. Conclusion

A numerical study was carried out to evaluate the effect of size of quadrilateral discontinuities on crashworthiness performance of square profiles. According to results obtained in the 'perfect' profile (ST-01), the implementation of both square, rectangular and diamond discontinuities, showed a reduction on peak load (P_{max}) value within a range of 0.77 – 25.97%. As the size of discontinuities grows, a reduction of peak value was registered independently of the initiator's shape. In all groups, the size of discontinuities determined the appearing of buckling effects at the beginning of the collapse of the profiles. It was observed that the reduction of the peak value (P_{max}) is influenced by the length of the major axis of the initiator in a major scale than in the minor axis. For discontinuities with a major axis length close to the width of the structure, the occurrence of hinge lines was faster and with less effort than discontinuities with denomination A and B. In all groups, the shape of the discontinuities is of great importance on peak load values from structures with denomination C holes (2.00 factor scale). With respect to energy absorption characteristics (E_a), the implementation of any type and size of discontinuities showed a better performance compared with a profile without discontinuities within a range of 2.74 – 12.54%. The values of E_a in all cases were increased until reaching an approximate maximum value of 2.86 kJ, after a decrease of E_a was noticed. A particular case was observed with structures III-E and III-F, which has a tendency to decrease E_a by increasing the size of initiator, these structures registered a second increase on energy absorption capabilities. Finally, it was found that the reduction of E_a capabilities resulted in partial deformations by buckling effect during the hinge line formation. This effect is major for structures with initiators with scale factors of 2.50, 3.00 and 3.50. For the specific case of profiles III-E and III-F it was observed that the relation between the minor axis and the major axis in addition to the diamond shape, have effects such as torsional and secondary deformations, improving the energy absorption characteristics (see fig. 20 and 21).

References

1. ABAQUS/Explicit User's Manual, Theory and examples manual and post manual. Version 5.8, Explicit, HKS, Inc., 1998.
2. Abramowicz W, Jones N. Dynamic axial crushing of circular tubes. International Journal of Impact Engineering 1984; 2(3): 263-281, http://dx.doi.org/10.1016/0734-743X(84)90010-1.
3. Aljawi A A N. Axial crushing of square steel tubes. The 6th Saudi Engineering Conference, KFUPM, Dhahran 2002; 3: 3-18.
4. Arnold B, Altenhof W. Experimental observations on the crush characteristics of AA6061 T4 and T6 structural square tubes with and without circular discontinuities. International Journal of Crashworthiness 2004; 9(1): 73-87, http://dx.doi.org/10.1533/ijcr.2004.0273.

5. Chenga Q, Altenhof W, Li L. Experimental investigations on the crush behaviour of AA6061-T6 aluminium square tubes with different types of through-hole discontinuities. Thin-Walled Structures 2006; 44(4): 441-454, http://dx.doi.org/10.1016/j.tws.2006.03.017.
6. Chiu Y S, Jenq S T. Crushing behaviour of metallic thin-wall tubes with triggering mechanisms due to quasi-static axial compression, Journal of the Chinese Institute of Engineers 2014; 37:4, 469:478.
7. Chung Kim Yuen S., Nurick G. N. The energy-absorbing characteristics of tubular structures with geometric and material modifications: An overview. ASME Applied Mechanics Reviews 2008; 61:020802, 1-15.
8. Ferdynus M. An energy absorber in the form of a thin-walled column with square cross-section and dimples. Eksploatacja i Niezawodnosc - Maintenance and Reliability 2013; 15 (3): 253-258.
9. Huang M Y, Tai Y S. Dynamic crushing characteristics of high strength steel cylinders with elliptical geometric discontinuities. Theoretical and Applied Fracture Mechanics 2010; 54(1): 44-53, http://dx.doi.org/10.1016/j.tafmec.2010.06.014.
10. Jensen O, Langseth M, Hopperstad O S. Experimental investigations on the behaviour of short to long square aluminium tubes subjected to axial loading. International Journal of Impact Engineering 2004; 30(8-9): 973-1003, http://dx.doi.org/10.1016/j.ijimpeng.2004.05.002.
11. Kim D K, Lee S. Impact energy absorption of 6061 aluminium extruded tubes with different cross-sectional shapes. Materials and Design 1999; 20(1): 41-49, http://dx.doi.org/10.1016/S0261-3069(98)00042-9.
12. Krauss C A, Lananen D H. A parametric study of crush initiators for a thin-walled tube. International Journal of Vehicle Design 1994; 15(3/4/5): 385-401.
13. Lee, S, Hahn C, Rhee M, Oh J E. Effect of triggering on the energy absorption capacity of axially compressed aluminum tubes. Mechanics and Design 1999; 20(1): 31-40, http://dx.doi.org/10.1016/s0261-3069(98)00043-0.
14. Mamalis A G, Manolakos D E, Spentzas K N, Ioannidis M B, Koutroubakis S, Kostazos P K. The effect of the implementation of circular holes as crush initiators to the crushing characteristics of mild steel square tubes: experimental and numerical simulation. International Journal of Crashworthiness 2009; 14(5): 489-50, http://dx.doi.org/10.1080/13588260902826547.
15. Matweb, http://www.matweb.com, 2014.
16. Peden M., Scurfield R., Sleet D., Mohan D., Adnan A. Hyder A. A., Eva Jarawan E. Mathers C., World report on road traffic injury prevention. Geneva, World Health Organization, 2004.
17. Simhachalam B, Krishna Srinivas K, Lakshmana Rao C. Energy absorption characteristics of aluminium alloy AA7XXX and AA6061 tubes subjected to static and dynamic axial load. International Journal of Crashworthiness 2014; 19(2): 139-152, http://dx.doi.org/10.1080/13588265.2013.878974.
18. Szwedowicz D, Estrada Q, Cortes C, Bedolla J, Alvarez G, Castro F. Evaluation of energy absorption performance of steel square profiles with circular discontinuities. Latin American Journal of Solids and Structures 2014; 11: 1744-1760, http://dx.doi.org/10.1590/S1679-78252014001000003.
19. Thornton, P. H., Mahmood, H. F., and Magee, C. L. Energy absorption by structural collapse. Structural Crashworthiness 1983, 96-117.
20. Wierzbicki T, Abramowicz W. On the crushing mechanics of thin-walled structures J. Appl. Mech 1983; 50(4a), 727-734, http://dx.doi.org/10.1115/1.3167137.
21. Zhang X, Huh H. Crushing analysis of polygonal columns and angle elements. International Journal of Impact Engineering. 2010; 37(4): 441-451, http://dx.doi.org/10.1016/j.ijimpeng.2009.06.009.

Quirino Estrada
Institute of Technology and Engineering
Autonomous University of Juarez City
Av. Plutarco Elías Calles 1210 C.P 32310, Ciudad Juarez, Chihuahua, Mexico

Dariusz Szwedowicz
Mechanical Engineering Department
National Center for Research and Technological Development
Internado Palmira S/N C.P 62490, Cuernavaca, Mor., Mexico

Tadeusz Majewski
Mechanical and Industrial Engineering Department
Universidad de las Americas
Cholula S/N C.P. 72810, Puebla, Mexico

Eladio Martinez
Mechanical Engineering Department
National Center for Research and Technological Development
Internado Palmira S/N C.P 62490, Cuernavaca, Mor., Mexico

Alejandro Rodriguez-Mendez
Department of Mechanical Engineering
University of California
Berkeley, CA 94720, USA

E-mails: quirino.estrada@uacj.mx, d.sz@cenidet.edu.mx,
tadeusz.majewski@udlap.mx, mare@cenidet.edu.mx, aleromende@berkeley.edu